White-light electroluminescence from ZnO nanorods/polyfluorene by solution-based growth

2009 Nanotechnology 20 425202

(http://iopscience.iop.org/0957-4484/20/42/425202)

Nanotechnology **20** (2009) 425202 (5pp) doi:10.1088/0957-4484/20/42/425202

White-light electroluminescence from ZnO nanorods/polyfluorene by solution-based growth

C Y Lee[1], J Y Wang[2], Y Chou[3], C L Cheng[2], C H Chao[1], S C Shiu[1], S C Hung[1], J J Chao[1], M Y Liu[1], W F Su[3], Y F Chen[2] and C F Lin[1,4]

[1] Graduate Institute of Photonics and Optoelectronics, National Taiwan University, Taipei 10617, Taiwan
[2] Department of Physics, National Taiwan University, Taipei 10617, Taiwan
[3] Graduate Institute of Materials Science and Engineering and Department of Materials Science and Engineering, National Taiwan University, Taipei 10617, Taiwan
[4] Graduate Institute of Electronics Engineering and Department of Electrical Engineering, National Taiwan University, Taipei 10617, Taiwan

E-mail: cflin@cc.ee.ntu.edu.tw

Received 8 June 2009, in final form 21 August 2009
Published 25 September 2009
Online at stacks.iop.org/Nano/20/425202

Abstract

We report bright white-light electroluminescence (EL) from a diode structure consisting of a ZnO nanorod (NR) and a p-type conducting polymer of poly(fluorine) (PF) fabricated using a hydrothermal method. ZnO NRs are successfully grown on an organic layer of PF using a modified seeding layer. The EL spectrum shows a broad emission band covering the entire visible range from 400 to 800 nm. White-light emission is possible because the ZnO-defect-related emission from the ZnO NR/PF heterostructure is enhanced to become over thousand times stronger than that from the usual ZnO NR structure. This strong green–yellow emission associated with the ZnO defects, combined with the blue PF-related emission, results in the white-light emission. Enhancement of the ZnO-defect emission is caused by the presence of $Zn(OH)_2$ at the interface between the ZnO NRs and PF. Fourier transform infrared spectroscopy reveals that the absorption peaks at 3441, 3502, and 3574 cm^{-1} corresponding to the OH group are formed at the ZnO NR/PF heterostructure, which confirms the enhancement of defect emission from the ZnO NR/PF heterostructure. The processing procedure revealed in this work is a convenient and low-cost way to fabricate ZnO-based white-light-emitting devices.

(Some figures in this article are in colour only in the electronic version)

Zinc oxide (ZnO) has attracted much attention as a solid-state lighting source with potential advantages over the III-nitride system due to the high exciton binding energy. In particular, ZnO nanostructures are very attractive for the possibility of their growth on alien substrates without the need for of lattice matching and utilizing various growth methods such as electron beam evaporation [1], spray pyrolysis [2], the solvothermal method [3], the sol–gel template method [4], hydrothermal decomposition [5], and so on. Recently, some researchers have reported the realization of ZnO light-emitting diodes through the above-mentioned methods [6, 7]. However, up to the present, only ZnO electroluminescence in the green to yellow or blue-UV region has been observed from homojunction or heterojunction nanostructures [8–10]. White-light electroluminescence from nanostructures has remained out of reach. In this work we report white-light electroluminescence from ZnO nanorod (NR)/poly(fluorine) (PF) heterostructure light-emitting diodes (LEDs) prepared by hydrothermal deposition at a low temperature of 90 °C with the ZnO NRs grown on the PF layer.

It is well known that undoped ZnO reveals n-type conduction [11] and the organic material PF exhibits p-type

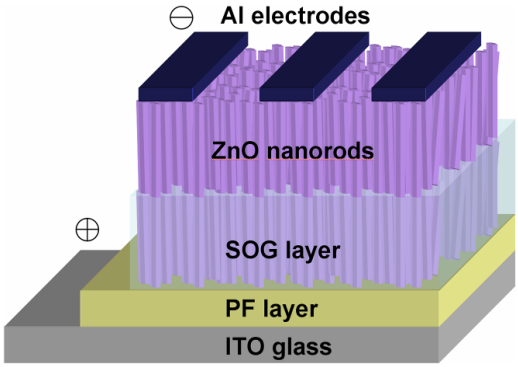

Figure 1. Schematic illustration of the ZnO NR/PF heterojunction white-light LED.

conduction [12], so these two materials form a p–n junction heterostructure for LEDs. Here we introduce a modified ZnO seeding layer so that ZnO NRs can be successfully grown on the PF thin film. The white-light electroluminescence is attributed to the greatly enhanced green–yellow emission associated with the ZnO surface defects at the ZnO NR/PF heterostructure and the blue emission from the PF. The color distribution covers the entire visible spectrum, extending from 400 to 800 nm. Our device structure provides a new approach to straightforward white-light electroluminescence devices which take advantage of the high carrier mobility of inorganic materials and the high luminescence efficiency of organic materials at very low cost.

A schematic diagram of the ZnO NR/PF heterostructure LED is shown in figure 1. Fabrication starts from the preparation of PF thin film on indium tin oxide (ITO)-coated glass by spin coating. To facilitate the nucleation of ZnO NR growth, a seeding layer consisting of 20 nm ZnO nanoparticles (NPs) is formed on top of the PF thin film by spin coating. Using the hydrothermal method, ZnO NRs are monolithically grown on top of the PF layer from an aqueous solution at a low temperature of 90 °C for 3 h. After deposition the NRs are rinsed in pure H_2O, dried in N_2, and then embedded in an insulating SOG (a polysiloxane-based dielectric material) layer that is spin coated from SOG solution. The SOG layer in the device is used to provide isolation for the individual ZnO NRs and prevent direct contact between the PF and the top electrode. Subsequently, oxygen plasma etching is used to remove SOG coated on top of the ZnO NRs to expose them for metallization. We confirm that the SOG filling is more effective at reducing surface leakage current than photoresist filling. An increase in the surface leakage of the LED would lead to weak performance. To ensure good contacts to each layer, the sample is then annealed at 120 °C for 2 h to remove the residual solvent. Finally, a 200 nm aluminum layer is deposited by thermal evaporation through a shadow mask to provide a contact for electron injection.

It is not easy to fabricate ZnO NRs on top of organic conducting materials because is difficult to form a good film of the general seeding solution, containing zinc acetate dihydrate, monoethanolamine, and 2-methoxyethanol (2MOE) [13], on top of organic conducting materials during spin coating. It

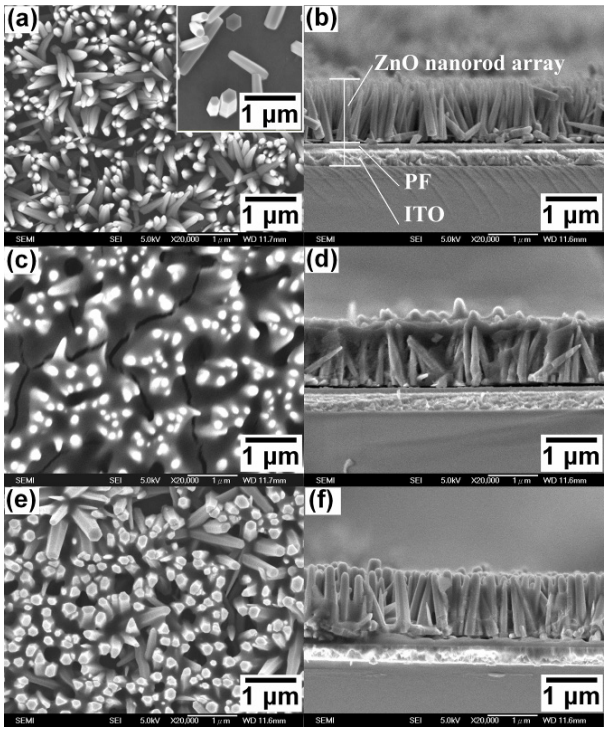

Figure 2. FESEM images from the different LED fabrications steps. (a) ZnO nanorods grown on PF thin film with a modified seeding layer (top view). (b) ZnO nanorods grown on PF thin film with a modified seeding layer (cross-sectional view). (Inset shows the growth of ZnO nanorods on PF without a modified seeding layer.) (c) ZnO nanorods spin-coated with SOG (top view). (d) ZnO nanorods spin-coated with SOG (cross-sectional view). (e) ZnO nanorods spin-coated with SOG after plasma treatment (top view). (f) ZnO nanorods spin-coated with SOG after plasma treatment (cross-sectional view).

is generally accepted that the role of the seeding layer is to supply ZnO nuclei to drive the precipitation reaction. In order to get good deposition of the seeding layer on top of the PF, we replace 2MOE with isopropyl alcohol (IPA) and add ZnO NPs to the seeding solution in the correct proportion. Then the modified seeding solution is heated to 120 °C. We have found that IPA is one of the few solvents that is compatible and innoxious to organic conducting materials. IPA allows the seeding solution to have good uniformity during spin coating. The addition of ZnO NPs leads to increased adsorbance of the seeding layer on top of the PF. The moderate heat treatment of the seeding solution improves the film-forming property of the seeding layer on top of PF by decreasing the surface tension of the seeding layer.

The morphology of ZnO NRs on top of the PF is examined using field-emission scanning electron microscopy (FESEM). Figures 2(a) and (b) show the top view and cross-sectional images, respectively, of the as-grown ZnO NRs with modified deposition of the seeding layer. The average length of the ZnO NRs and the thickness of the PF layer are about 1.25 μm and 90 nm, respectively. The ZnO NRs are well aligned and dense on top of PF with an average diameter of about 120 nm. In contrast, as seen in the inset of figure 2(a), the NRs grown without the modified seeding layer show striking

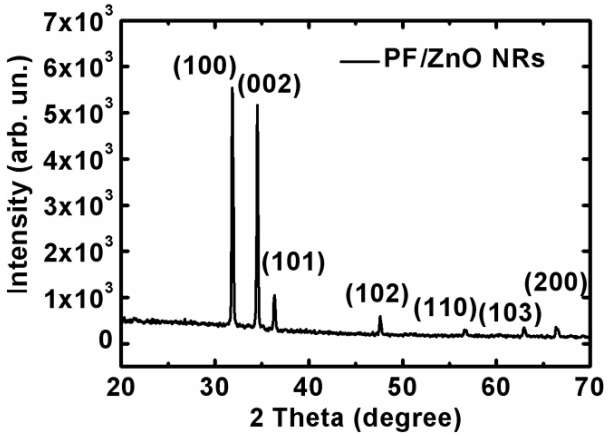

Figure 3. XRD pattern of ZnO nanorods on PF prepared by the hydrothermal method at 90° for 3 h using zinc nitrate as the zinc source.

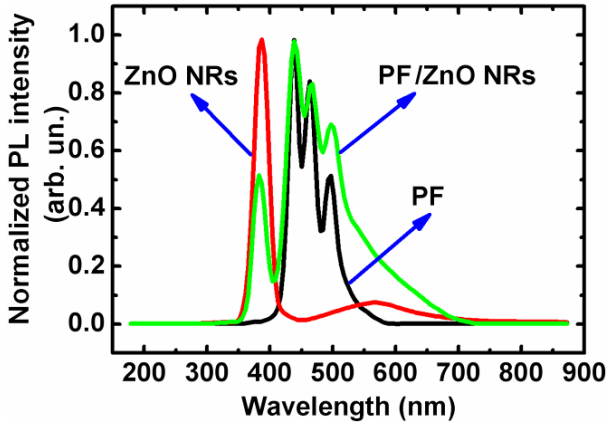

Figure 4. Normalized photoluminescence spectra of (a) PF thin film, (b) ZnO nanorods, and (c) PF/ZnO seeding layer/ZnO nanorods.

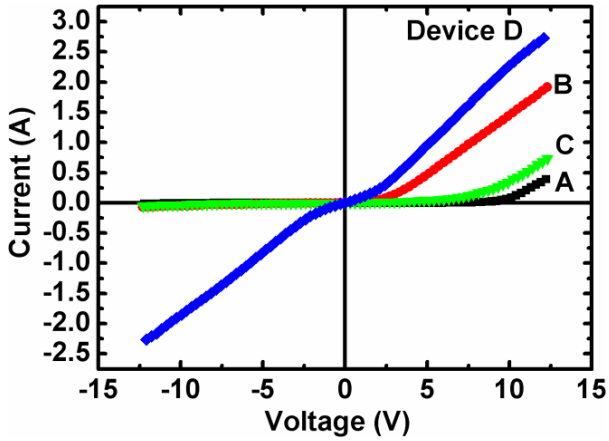

Figure 5. The room temperature I–V curves in the dc bias mode for (a) ITO/PF/Al, (b) ITO/PF (90 nm)/ZnO seeding layer/ZnO NRs:SOG/Al, (c) ITO/PF (240 nm, thick)/ZnO seeding layer/ZnO NRs:SOG/Al, and (d) ITO/ZnO NRs:SOG/Al.

changes of density and size, indicating that the density and size of the ZnO NRs depend strongly on the modified seeding layer. Figures 2(c) and (d) show that a thin SOG coating on top of the NRs can be achieved. The space between the NRs is solidly filled with SOG. The ZnO NRs:SOG on PF after oxygen plasma treatment are shown in figures 2(e) and (f). The bright spots are the ZnO NRs and the dark area is the space between the NRs filled with SOG.

The XRD pattern of the ZnO NRs on PF is obtained using an x-ray diffraction meter with Cu Kα radiation (λ = 0.154 06 nm) operated at 40 kV and 25 mA. As shown in figure 3, several diffraction peaks could be observed at 2θ = 31.74°, 34.44°, 36.26°, 47.48°, 56.66°, and 62.93°, which are due to ZnO(100), (002), (101), (102), (110), and (103), respectively [14]. All of these peaks match the wurtzite ZnO structure (JCPDS card no. 36-1451). The strong clear peaks reveal the crystallinity of the ZnO NRs on top of the PF.

Figure 4 shows the normalized photoluminescence (PL) spectra of the ZnO NRs, ZnO NRs/PF, and PF thin film at room temperature. The PL spectrum of the ZnO NR/PF heterostructure can be clearly identified by two clear emission bands with a long tail. The long tail in green–yellow emission from 520 to 720 nm and an UV emission band at 380 nm are from surface defects of ZnO NRs and excitonic emission of ZnO NRs, respectively. The blue emission band with peaks at 440, 465, and 495 nm is attributed to PF-related emission.

The current–voltage characteristics of the EL devices at room temperature are shown in figure 5. Four kinds of device with different structures, ITO/PF/Al (device A), ITO/PF (90 nm)/ZnO NRs:SOG/Al (device B), ITO/PF (240 nm, thick)/ZnO NRs:SOG/Al (device C), ITO/ZnO NRs:SOG/Al (device D), were fabricated for comparison. Devices B and C have a ZnO NR:SOG/PF double-layer structure (p–n junction) while devices A and D are single-layer devices. For the double-layer devices, devices B and C demonstrate reasonable p–n junction characteristics. In device C, because the PF layer is too thick, the corresponding current–voltage curve reveals a relatively lower current density than the ZnO-based device with a 90 nm thickness of PF (device B). For the single-layer devices, the current–voltage curves of device A are similar to those of devices B and C, but the rectification characteristic of device A is not as good as those of devices B and C. That is to say, the current of device A is lower than those of devices B and C at a given voltage. From the above results, the device with ZnO NRs shows a higher current density at the same voltage and a relatively lower driving voltage than the device without ZnO NRs (device A). We attribute this phenomenon to a higher carrier mobility of ZnO NR/PF heterostructure than that of PF film only. As for device D, the curve indicates that the ZnO NRs directly contact the ITO substrate, leading to the large current leakage.

Figure 6(a) shows the EL spectra of devices A, B, C, and D at room temperature under a forward dc bias of 10 V. For the single-layer devices with only PF as the light emission material, device A displays three blue EL emission peaks at 433, 452, and 490 nm that correspond to the PF emission, which agrees with most LED reports [15, 16]. As for device D, a broad defect-related emission centered at 567 nm is observed, which is similar to the results previously reported for ZnO EL devices by different authors [17, 18]. For the double-layer

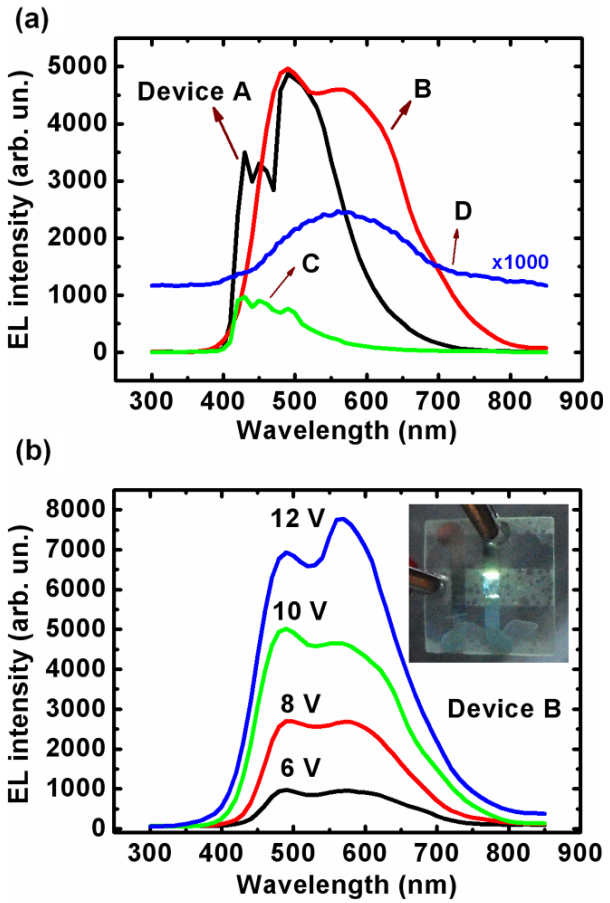

Figure 6. (a) The room temperature EL spectra of all devices in the dc bias mode under a forward bias of 10 V. (b) The room temperature EL spectra of device B in the dc bias mode under different applied voltages. (The inset is a photograph of light emission from device B under a forward bias of 10 V.)

devices, a white-light emission consisting of a broad green–yellow emission centered at 567 nm and a blue emission at 489 nm is observed in device B.

A comparison of device B with devices A and D reveals that the broad green–yellow band comes from surface defects of ZnO NRs, while the blue band results from the PF-related emission. The emissions suggested that carrier recombination should take place in the ZnO NR/PF interface. It is interesting to note that the EL spectrum of device B is very different from those previously reported in ZnO inorganic/organic heterostructure devices, where the emissions are from either ZnO only [19, 20] or the organic layer only [1]. The high intensity of green–yellow emission and quenching of UV emission from ZnO NRs in the ZnO NR/PF heterostructure can be explained by the hydrothermal process. It is known that ZnO NRs grown by the solution method present a large number of defects [21, 22], which are reflected by both PL and EL. During the synthesis, the presence of OH groups results in the formation of $Zn(OH)_2$ on the surface of ZnO NRs. The $Zn(OH)_2$ will quench the UV emission and enhance the surface defect emission [23]. Meanwhile, the interaction between the ZnO surface and the PF molecules makes the PF link up with ZnO. This leads to the ZnO NR/PF interface producing a strong defect emission. As a result, the EL spectrum of device B ranges from 400 to 800 nm and gives rise to the white color of the emission.

In order to further understand the conditions of white-light emission, we increase the thickness of the PF to 240 nm (device C). Device C shows only blue band emission, which corresponds to the PF-related emission only. This indicates that carrier recombination mainly occurs in the PF layer. The thick PF layer (240 nm) provides a long conductive path for holes. Besides, the mobility of electrons in the ZnO NRs is higher than that of holes in the PF layer. Thus the recombination zone of holes and electrons is restricted to the PF layer. Obviously, the differences in the EL spectrum between device B and device C are due to differences in the emission mechanism, which results from differences in the position of the recombination region. In addition it is worth mentioning that the EL intensity of the ZnO NR/PF structure (device B) is at least three orders of magnitudes larger than that of the ZnO NR/ITO structure (device D). The brightness measured in device B under 10 V is over 100 nits. This result demonstrates a good route for realizing a ZnO-based white-light LED by combining ZnO NRs with a high luminescence polymer.

EL spectra of device B were further measured at various applied forward-bias voltages from 6 to 12 V, as shown in figure 6(b.) At applied voltages below 10 V, the EL emission peaks are observed at 489 and 567 nm without exhibiting a spectral shift. The inset in figure 6(b) is a photograph of white-light EL from device B under a forward bias of 10 V. The Commission International de l'Eclairage (CIE) coordinate is (0.30, 0.34) which is quite stable with varying applied biases from 6 to 10 V, exhibiting variations of less than 5%. As the applied voltage reaches 12 V, the emission at the green–yellow band increases more than the blue band because of more excitation to the ZnO surface defects. However, for further increases in applied voltage over 12 V the device is broken-down, which results in no EL.

Fourier transform infrared spectroscopy (FTIR) is used to investigate the origins of the ZnO-defect associated emissions. To avoid the contribution from the ITO-coated glass, special samples with the PF film, film of the PF/ZnO seeding layer and film of the PF/ZnO seeding layer/ZnO NRs were prepared on salt substrates and then the salt substrates were removed by dissolving in de-ionized water. In this way the characteristics of the ZnO NR/PF heterostructure can be better clarified by FTIR spectroscopy. Figure 7 shows the FTIR spectra of the ZnO NR/PF heterostructure in each phase of its preparation procedure. In spectrum (a) (PF film), absorption peaks at 2953, 2926, 2855, 1460, 1402, 1377, 1253, 1123, and 813 cm^{-1} are characteristics of PF molecular vibration, in good agreement with published spectra [24]. Compared to spectrum (a), spectrum (b) (PF/ZnO seeding layer) reveals the shift in some absorption peaks, a decrease in the transmission intensity of each absorption peak, and the appearance of a new shoulder at 3400–3600 cm^{-1} of the OH stretching band, showing the formation of a new phase on the interface between the ZnO seeding layer and the PF film. In spectrum (c) (PF/ZnO seeding layer/ZnO NRs), three new characteristic peaks appear at 3441,

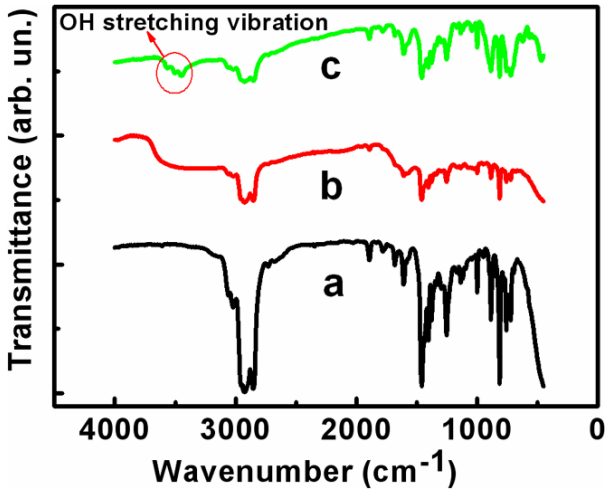

Figure 7. FTIR spectra of (a) PF thin film, (b) PF/ZnO seeding layer, and (c) PF/ZnO seeding layer/ZnO NRs.

3502, and 3574 cm^{-1}, which are assigned to the OH stretching band [25]. The results confirm the presence of OH groups on the ZnO NR/PF heterostructure. The presence of OH groups is expected to result in the formation of a $Zn(OH)_2$ defect [23]. Hence, the ZnO NR/PF heterostructure provides strong defect centers.

In conclusion, a ZnO NR/PF inorganic/organic heterostructure white-light LED has been reported. The device shows a broad band emission, which corresponds to the significantly enhanced ZnO surface defect emission and PF-related emission, respectively. The white-light electroluminescence covering the spectral range from 400 to 800 nm is caused by carrier recombination at the interface between ZnO NRs and PF as well as in the PF film. FTIR spectra reveal OH groups at 3441, 3502, and 3574 cm^{-1} on the ZnO NR/PF heterostructure, which confirms the enhancement of surface defects from the ZnO NR/PF heterostructure. We believe that the results in this work provide a significant step toward the realization of ZnO-based white-light EL devices with low-temperature processes for potential large-scale production at a very cost in the future.

Acknowledgments

This work is supported by the National Science Council, Taiwan, Republic of China, with grant no. NSC96-2221-E-002-277-MY3, NSC97-2218-E-002-013, and NSC97-2221-E-002-039-MY3.

References

[1] Huang F, Xu Z, Zhao S, Li Y, Zhang F, Song L, Wang Y and Xu X 2007 *Solid State Commun.* **142** 417–20
[2] Bolink H J, Coronado E and Sssolo M 2009 *Chem. Mater.* **21** 439–41
[3] Cheng H M, Chiu W H, Lee C H, Tsai S Y and Hsieh W F 2008 *J. Phys. Chem.* C **112** 16359–64
[4] Ning G H, Zhao X P, Li J and Zhang C Q 2006 *Opt. Mater.* **28** 385–90
[5] Wong C Y, Lai L M, Leung S L, Roy V A L and Pun E Y B 2008 *Appl. Phys. Lett.* **93** 023502
[6] Xi Y Y, Hsu Y F, Djurišić A B, Ng A M C, Chan W K, Tam H L and Cheah K W 2008 *Appl. Phys. Lett.* **92** 113505
[7] Yan C, Chen Z and Zhao X 2006 *Solid State Commun.* **140** 18–22
[8] Yang Y, Sun X W, Tay B K, You G F, Tan S T and Teo K L 2008 *Appl. Phys. Lett.* **93** 253107
[9] Zhang X M, Lu M Y, Zhang Y, Chen L J and Wang Z L 2009 *Adv. Mater.* **21** 1–4
[10] Lee C Y, Hui Y Y, Su W F and Lin C F 2008 *Appl. Phys. Lett.* **92** 261107
[11] Sun J C, Zhao J Z, Liang H W, Bian J M, Hu L Z, Zhang H Q, Liang X P, Liu W F and Du G T 2007 *Appl. Phys. Lett.* **90** 121128
[12] Izard N, Kazaoui S, Hata K, Okazaki T, Saito T, Iijima S and Minami N 2008 *Appl. Phys. Lett.* **92** 243112
[13] Baruah S and Dutta J 2009 *Sci. Technol. Adv. Mater.* **10** 013001
[14] Ghosh M, Bhattacharyya R and Raychaudhuri A K 2008 *Bull. Mater. Sci.* **31** 283–9
[15] Cho S Y, Grimsdale A C, Jones D J, Watkins S E and Holmes A B 2007 *J. Am. Chem. Soc.* **129** 11910–1
[16] Zhu Y, Gibbons K M, Kulkarni A P and Jenekhe S A 2007 *Macromolecules* **40** 804–13
[17] Nadarajah A, Word R C, Meiss J and Könenkamp R 2008 *Nano Lett.* **8** 534–7
[18] Könenkamp R, Word R C and Schlegel C 2004 *Appl. Phys. Lett.* **85** 6004–6
[19] Sun X W, Huang J Z, Wang J X and Xu Z 2008 *Nano Lett.* **8** 1219–23
[20] Könenkamp R, Word R C and Godinez M 2005 *Nano Lett.* **5** 2005–8
[21] Yang J H, Zheng J H, Zhai H J and Yang L L 2009 *Cryst. Res. Technol.* **44** 87–91
[22] Ahsanulhaq Q, Umar A and Hahn Y B 2007 *Nanotechnology* **18** 115603
[23] Yadav H K, Sreenivas K and Gupta V 2007 *J. Mater. Res.* **22** 2404–9
[24] Zhao W, Cao T and White J M 2004 *Adv. Funct. Mater.* **14** 783–90
[25] Wang J, Zhang S, You J, Yan H, Li Z, Jing X and Zhang M 2008 *Bull. Mater. Sci.* **31** 597–601